

# 3.4- $\mu\text{m}$ ZGP RISTRA nanosecond optical parametric oscillator pumped by a 2.05- $\mu\text{m}$ Ho:YLF MOPA system

Alex Dergachev<sup>1\*</sup>, Darrell Armstrong<sup>2</sup> and Arlee Smith<sup>2</sup>,  
Thomas Drake<sup>3</sup> and Marc Dubois<sup>3</sup>

<sup>1</sup>*Q-Peak, Inc., 135 South Road, Bedford, Massachusetts 01730*

<sup>2</sup>*Department 1128, Sandia National Laboratories, Albuquerque, New Mexico 87185-1423*

<sup>3</sup>*Lockheed Martin Aeronautics Company, One Lockheed Blvd. MZ 6852 Bldg.4 22C, Fort Worth, Texas 76108*

\*Corresponding author: [dergachev@qpeak.com](mailto:dergachev@qpeak.com)

**Abstract:** We report on the first demonstration of ZGP OPO based on Rotated Image Singly-Resonant Twisted RectAngle (RISTRA) cavity. For the OPO signal wave we achieved a near diffraction-limited beam at 3.4  $\mu\text{m}$  with pulse energy of 10 mJ at repetition rate up to 500 Hz. As a pump source for the ZGP OPO, we utilized a 2- $\mu\text{m}$ , TEM<sub>00</sub>, Ho:YLF MOPA system producing > 55 mJ energy per pulse at repetition rate range from single shot to 500 Hz.

©2007 Optical Society of America

OCIS codes: (190.4970) Parametric oscillators and amplifiers; (140.3580) Lasers, solid-state

## References and links

1. P. A. Budni, L. A. Pomeranz, M. L. Lemons, C. A. Miller, J. R. Mosto, and E. P. Chicklis, "Efficient mid-infrared laser using 1.9- $\mu\text{m}$ -pumped Ho:YAG and ZnGeP<sub>2</sub> optical parametric oscillator," *J. Opt. Soc. Am. B* **17**, 723–728 (2000).
2. K. L. Vodopyanov, F. Ganikhanov, J. P. Maffetone, I. Zwieback, and W. Ruderman, "ZnGeP<sub>2</sub> optical parametric oscillator with 3.8–12.4- $\mu\text{m}$  tunability," *Opt. Lett.* **25**, 841–843 (2000).
3. V. G. Dmitriev, G. G. Gurzadyan, and D. N. Nikogosyan, *Handbook of nonlinear optical crystals* (Springer-Verlag, 1997).
4. P. A. Budni, C. R. Ibach, S. D. Setzler, L. A. Pomeranz, M. L. Lemons, P. A. Ketteridge, E. J. Gustafson, Y. E. Young, P. G. Schunemann, T. M. Pollak, R. T. Castro, and E. P. Chicklis, "20-mJ, 3-5 micron ZnGeP<sub>2</sub> optical parametric oscillator pumped by a 2.09-micron Ho:YAG laser," in *Advanced Solid State Photonics*, Technical Digest (Optical Society of America, 2003), paper PD12-1.
5. E. Lippert, S. Nicolas, G. Arisholm, K. Stenersen, and G. Rustad, "Midinfrared laser source with high power and beam quality," *Appl. Opt.* **45**, 3839-3845 (2006).
6. D. Gapontsev, N. Platonov, M. Meleshkevich, A. Drozhzhin, V. Sergeev, "415 W Single-Mode CW Thulium fiber laser in all-fiber format", in *CLEO-Europe 2007*, Technical Digest, paper CP2-3-THU.
7. P. A. Budni, C. R. Ibach, S. D. Setzler, E. J. Gustafson, R. T. Castro, and E. P. Chicklis, "50-mJ, Q-switched, 2.09- $\mu\text{m}$  holmium laser resonantly pumped by a diode-pumped 1.9- $\mu\text{m}$  thulium laser," *Opt. Lett.* **28**, 1016-1018 (2003).
8. M. Petros, J. Yu, U. N. Singh, and N. P. Barnes, "High energy directly pumped Ho:YLF laser," in *Advanced Solid State Lasers*, OSA Trends in Optics and Photonics Vol. 34, (Optical Society of America, 2000), pp. 178-181.
9. A. Dergachev, P.F. Moulton, "High-power, high-energy diode-pumped Tm:YLF-Ho:YLF-ZGP laser system", in *Advanced Solid-State Photonics*, OSA Trends in Optic and Photonics Vol. 83, (Optical Society of America, 2003), pp. 137-141.
10. A. Dergachev, P. F. Moulton, and T. E. Drake, "High-power, high-energy Ho:YLF laser pumped with Tm: fiber laser", in *Advanced Solid-State Photonics*, OSA Trends in Optic and Photonics Vol. 98, (Optical Society of America, 2005), pp. 608-612.
11. A. V. Smith and D. J. Armstrong, "Nanosecond optical parametric oscillator with 90° image rotation: design and performance," *J. Opt. Soc. Am. B* **19**, 1801–1814 (2002).
12. D. J. Armstrong and A. V. Smith, "90% pump depletion and good beam quality in a pulse-injection-seeded nanosecond optical parametric oscillator," *Opt. Lett.* **31**, 380–382 (2006).
13. D. J. Armstrong and A. V. Smith, "All solid-state high-efficiency tunable UV source for airborne or satellite-based ozone DIAL systems," *IEEE J. Sel. Top. Quantum Electron.* **13**, 721–731 (2007).

14. D. J. Armstrong and A. V. Smith, "150-mJ 1550-nm KTA OPO with good beam quality and high efficiency," Proc. SPIE **5337**, 71-80 (2004).
  15. D. J. Armstrong and A. V. Smith, "Using a Newport refractive beam shaper to generate high-quality flat-top spatial profiles from a flashlamp-pumped commercial Nd:YAG laser," Proc. SPIE **5525**, 88-97 (2004).
  16. <http://www.sandia.gov/imrl/XWEB1128/xxtal.htm> A complete package of numerical models for crystal nonlinear optics is available in the SNLO software package from A. V. Smith at Sandia National Labs. Models for the RISTRA OPO are available on request.
  17. A. V. Smith, W. J. Alford, T. D. Raymond, and M. S. Bowers, "Comparison of a numerical model with measured performance of a seeded, nanosecond KTP optical parametric oscillator," J. Opt. Soc. Am. B **12**, 2253-2267 (1995).
  18. G. Anstett, M. Nittman, and R. Wallenstein, "Experimental investigation and numerical simulation of the spatio-temporal dynamics of the light-pulses in nanosecond optical parametric oscillators," Appl. Phys. B, **79**, 305-313 (2004).
  19. A. V. Smith and D. J. Armstrong, "Generation of vortex beams by an image-rotating optical parametric oscillator," Opt. Express **11**, 868-873 (2003).
- 

## 1. Introduction

OPOs based on the crystal ZnGeP<sub>2</sub> (ZGP) are widely used for generating tunable IR radiation in the 2.5-12- $\mu\text{m}$  region [1-5]. ZGP crystal possesses a set of unique properties such as high nonlinearity ( $d_{36}=75 \pm 8$  pm/V), high thermal conductivity of 35-36 W/(m K) (higher than YAG) and relatively high hardness 5.5 (Mohs scale) [3].

ZGP requires a pump wavelength longer than 2  $\mu\text{m}$  with typical sources being the 2- $\mu\text{m}$  Ho-lasers and 3- $\mu\text{m}$  Er-lasers. ZGP OPOs are usually operated either at low repetition rates < 60 Hz with mJ-pulse energies [2, 4] or at repetition rates >10 kHz with maximum pulse energies of 100s of  $\mu\text{J}$  [1, 5].

A significant drawback of ZGP crystals (as well as other non-linear crystals used for IR generation) is a low damage threshold of <1-2 J/cm<sup>2</sup> for nanosecond pulses. Nanosecond OPOs operating at pulse energy in 10-100-mJ range require large diameter pump beams to safely extract high energy levels without the risk of optical damage to the crystal. Conventional standing-wave or planar-ring OPO cavities operating with high cavity Fresnel numbers ( $N_F = D^2/\lambda L$ , where  $D$  is the beam diameter,  $\lambda$  is the OPO signal wavelength and  $L$  is the cavity length) produce low-quality beams. Our ZGP OPO uses a non-planar geometry, where the cavity's image rotation, working in conjunction with crystal birefringence, significantly improves the spatial quality of the beam. However, to achieve high optical efficiency and produce the best beam quality, an OPO cavity design is not sufficient by itself: the pump laser must also be efficient and have a high beam quality as well.

In this particular effort, we applied the Rotated Image Singly-Resonant Twisted RectAngle (RISTRA) concept to construct a mid-IR ZGP OPO to produce a 3.4- $\mu\text{m}$  signal wave with > 10 mJ of energy with a near diffraction-limited beam quality.

ZGP OPO was pumped by a pulsed 2.05- $\mu\text{m}$  master-oscillator power-amplifier (MOPA) Ho:YLF system. We used a Tm-fiber-laser-pumped MOPA approach to scale the output of a 2.05- $\mu\text{m}$  Q-switched Ho:YLF laser oscillator to pulse energies > 55 mJ at the rates from single shot to 500 Hz (38 mJ at 1 kHz).

## 2. Ho:YLF master-oscillator/ power-amplifier

As a pump source for the Ho:YLF MOPA system we utilized a single-mode >100-W Tm-fiber laser (Model TLR-100-1940, commercially available from IPG Photonics (Oxford, MA)) which was wavelength-adjusted to the strongest Ho:YLF absorption line at 1940 nm. The fiber laser was operated in CW regime and produced diffraction-limited output beam with maximum average power of 120 W. The <3-nm linewidth of the Tm-fiber laser was sufficiently narrow to match the 1940-nm absorption line in Ho:YLF.

Recent progress in the development and commercialization of Tm-fiber lasers providing high CW output power (up to 415 W) [6], diffraction-limited beam quality, and wide operating wavelength range, makes these lasers ideal pump sources for Ho-doped lasers and laser systems. Tm-fiber lasers can be wavelength-tuned to match any Ho-doped laser material

with the most common being Ho:YAG [1,4-5] and Ho:YLF [8-10]. Tm-fiber lasers seem to be a preferred alternative to bulk Tm-doped lasers for pumping applications demanding diffraction-limited CW power greater than 25-50 W.

We have chosen Ho:YLF as the gain medium for our system because of the combination of a high gain cross-section and long storage time of the Ho-transition and the athermal and birefringent nature of the YLF crystal, all advantages compared to Ho:YAG and other Ho-doped gain media.

The layout of the Ho:YLF master oscillator and single amplifier stage is shown in Fig. 1. (The Ho:YLF oscillator design follows closely that reported in Ref. [9].) The collimated output beam from the Tm-fiber laser was split into two orthogonally polarized beams using a polarizing beam splitter. A half-wave plate was used to rotate the polarization of the transmitted beam by  $90^\circ$ . One of the split beams was used to pump the master oscillator and the other to pump the amplifier stage. Each Ho:YLF laser crystal could be pumped with up to 60 W of CW power at 1940 nm. TEM<sub>00</sub> operation was assured by adjusting the pump beam diameter in the Ho:YLF crystals slightly smaller than the fundamental-mode size of the Ho:YLF laser cavity. To allow for a higher pulse energy in the Q-switched regime, the design strategy for the Ho:YLF MOPA was to maximize the laser mode size in order to reduce the possibility of optical damage.

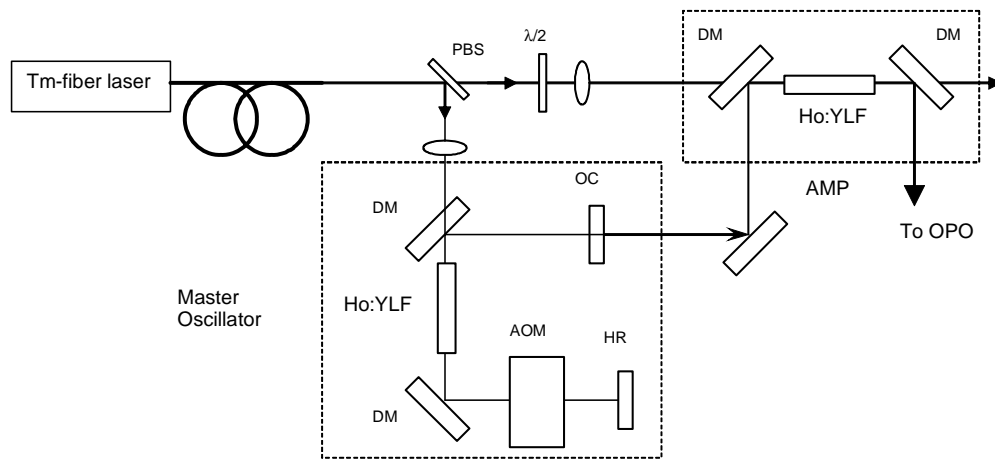


Fig. 1. Schematic layout of the end-pumped Ho:YLF MOPA (PBS – polarizing beam splitter, DM – Dichroic Mirror, AOM – Acousto-Optic Modulator, OC – Output Coupler, HR – High Reflector).

The Ho:YLF crystals in the master oscillator and amplifier stage were operated at room temperature. When the oscillator was optimized for Q-switched operation, maximum output power with a 70% -transmissive output coupler was  $\sim 19$  W at  $\sim 60$  W of Tm-pump power corresponding to 32% optical-to-optical efficiency. (The same oscillator optimized for CW operation produced 25-26 W corresponding to 42% optical-to-optical efficiency). An acousto-optic modulator was used to Q-switch the Ho:YLF laser. The output pulse energy and pulsewidth at two different repetition rates vs. Tm-fiber pump power are plotted in Fig.2. The minimum pulsewidth was  $\sim 14$  ns at the highest pulse energy. The master oscillator determined the repetition rate, pulsewidth and beam quality of the whole MOPA system. The MOPA operation was monitored in CW regime and at 500 Hz and 1000 Hz in the Q-switched regime. In principle, the repetition rate could be continuously adjusted from single shot to 100 kHz.

The Ho:YLF amplifier stage was operated in a fully saturated regime and allowed to extract  $\sim 23$  W in CW regime, and  $\sim 20$  mJ (1000 Hz) or  $\sim 30$  mJ (up to 500 Hz) in the Q-switched regime. The output beam from the Ho-MOPA was the lowest order Gaussian mode.

It is necessary to point out that Ho-lasers operate as quasi-4 level systems. When not pumped the laser material exhibits loss at the laser wavelength due to the ground state

absorption. In order to achieve gain the ground state absorption should be bleached by the pump beam with the gain region acting as a soft aperture. This soft-aperture effect significantly simplifies the generation of the lowest order beams: 1) the higher-order modes are effectively suppressed from propagating in the oscillator cavity and 2) the modulation of the beam profile due to diffraction on the amplifier rod apertures is not present.

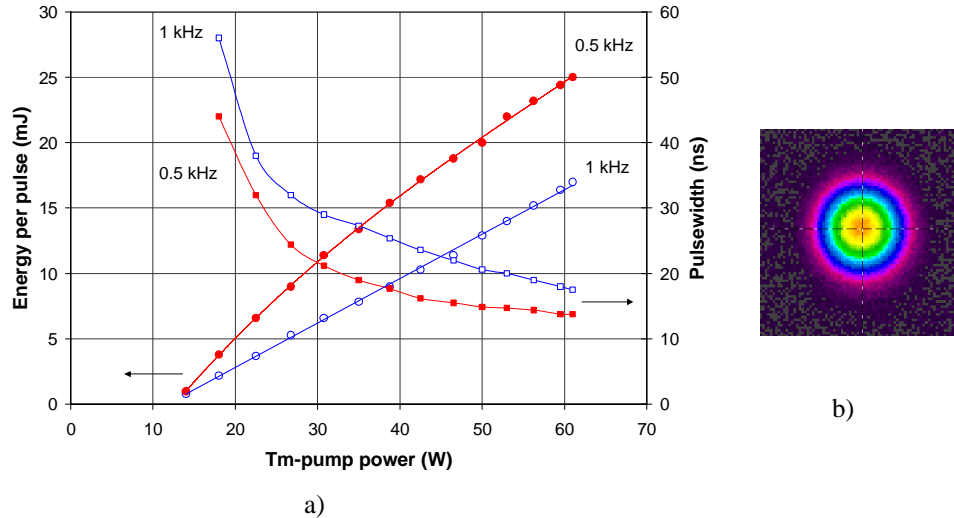


Fig. 2. (a). Energy per pulse and pulsewidth for Ho:YLF master oscillator vs. pump power (TEM<sub>00</sub> operation). (b) Oscillator beam profile at 500 Hz.

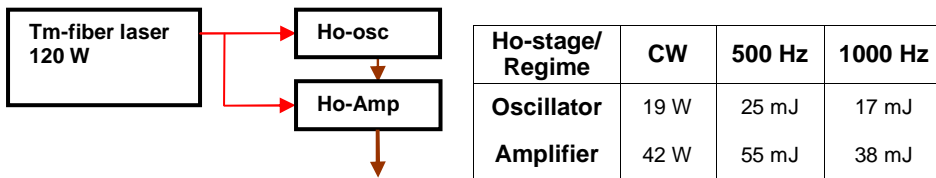


Fig. 3. Block-diagram of Ho-MOPA system and the table detailing the pertinent parameters for each stage.

The Ho:YLF MOPA beam size was adjusted with a two-lens collimator to limit the peak energy density in the OPO crystal below  $\sim 1.0 \text{ J/cm}^2$  at 60 mJ. This assured damage-free operation of ZGP crystal.

### 3. ZGP RISTRA OPO

The OPO for our mid-IR system used a 10-mm-long ZGP crystal obtained from Inrad, Inc. (Northvale, NJ). The crystal was AR-coated on both sides to minimize reflections at the pump, signal and idler wavelengths.

The OPO resonator is based on a four-mirror non-planar image-rotating ring cavity known as the RISTRA [11]. This cavity design was selected because intra-cavity image rotation can generate highly symmetric, high quality output beams under operating conditions that would otherwise lead to very poor beam quality. As explained in Ref. [11], image rotation works in conjunction with angle critical birefringent phase matching to increase phase front correlation across the beam profile, and it also introduces spatial averaging. Image rotation is particularly effective for improving beam quality in higher energy ns OPOs, where the ratio of beam diameter to cavity length results in a cavity Fresnel number that can be intentionally large. In

optical cavities  $N_F$  provides a measure of the number of Fresnel zones and indicates the strength of diffractive coupling, so that small  $N_F$  results in good beam quality, while large  $N_F$  tends to result in very poor beam quality. For example, with the RISTRA's physical length of  $\sim 109$  mm  $N_F$  can exceed several hundred for visible to near-IR wavelengths and pump beam diameters of 6 – 8 mm. For non-image-rotating ns OPOs  $N_F \geq 100$  is usually a recipe for very poor beam quality, however the RISTRA can deliver good beam quality for  $N_F \geq 400$  [12, 13], and it has generated a 1550-nm signal beam with  $M^2 \approx 4$  for pulse energies of 150 mJ [14].

An additional benefit of the RISTRA design, which is shown in Fig. 4(a), is that ring cavities having non-planar geometry are insensitive to small tilts of their cavity mirrors [11]. Tilting a mirror repositions the cavity's unique axis, which in turn might require repositioning the pump beam, and also the seed beam for injection seeded operation, but the cavity's properties remain unchanged. Consequently the RISTRA can be engineered as a quasi-monolithic cylinder with no mirror adjustments, as shown in Fig. 4(b). This mechanically robust design is highly stable, exhibits excellent pointing stability, and lends itself to applications where vibration may perturb conventional cavities having comparable rigidity, especially those requiring injection seeding and frequency stabilization. Owing to the monolithic structure and a desire to keep the cavity as short as practical, the diameter of the cavity bores in a standard-size RISTRA cylinder is limited to 10 mm, and crystal apertures to  $10 \times 10$  mm<sup>2</sup>, so that the largest practical pump beam diameter is  $\leq 8$  mm for a flat-top spatial profile. Other pump-beam spatial profiles such as Gaussians are acceptable, however, care must be taken so their wings are not clipped by 10-mm aperture. Because the RISTRA was designed for high pulse energies, flat-topped pump profiles are generally the best choice, where the uniform strength of non-linear mixing enhances efficiency and helps maintain peak fluences below the thresholds for optical damage to crystals and coatings. Conventional OPO cavities can accommodate large diameter beams as well, but the resulting high Fresnel numbers lead to an inevitable reduction in beam quality.

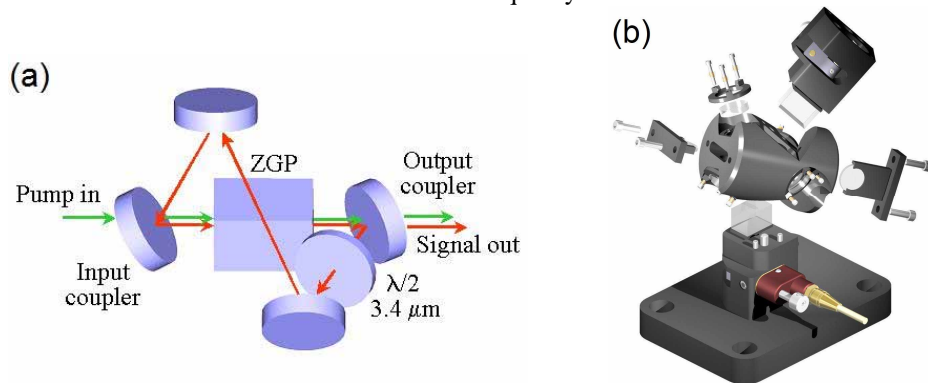


Fig. 4. (a). Geometric configuration of the RISTRA OPO cavity. The two long legs can hold crystals with apertures up to  $10 \times 10$  mm<sup>2</sup> and length  $\leq 17$  mm and the two short legs contain  $\lambda/2$ -retardation plates to orient cavity polarizations parallel to the eigen-polarizations of the crystals. The ratio of the physical lengths of the cavity legs is  $\sqrt{2}$ . The angle of incidence on all cavity mirrors is  $32.765^\circ$ , and the nominal physical length of the cavity is 109 mm. In this figure the cavity contains one crystal and one  $\lambda/2$ -plate. For a two-crystal cavity the waveplate in the short horizontal leg must have retardation of  $\lambda/2$  for the pump and resonated wave, and a second  $\lambda/2$ -plate is added to the short vertical leg. For our experiments the length of the ZGP crystal is 10 mm and the signal wavelength is 3.4  $\mu\text{m}$ . The output coupler reflectivity is  $\sim 50\%$ . (b) Exploded solid rendering of a two-crystal RISTRA cavity assembly showing cylindrical body, spring-loaded three-point mirror retainers and mirror substrates, waveplate holders, and crystal rotation assemblies. Owing to its non-planar geometry the RISTRA requires no cavity mirror adjustments. The length of the cylinder is 50 mm, and the mirror substrates have diameters of 12.5 mm and thickness of 3 mm. See text for additional details.

In previously reported applications of the RISTRA cavity the OPO was injection seeded for single frequency oscillation, and it was pumped by the first or second harmonic of a single-frequency injection-seeded Nd:YAG laser that had a high-quality flat-topped spatial profile [15]. An important difference for the mid-IR system described here, aside from using ZGP and having longer pump, signal, and idler wavelengths, is that OPO and pump laser both oscillate on multiple longitudinal modes. Although ns OPOs are commonly pumped by broadband lasers and operate without injection seeding and frequency stabilization, this is the first reported application of the RISTRA OPO where its performance was evaluated under these conditions. These differences are significant because broadband oscillation affects conversion efficiency and beam quality, and previously the RISTRA OPO was characterized only for single-frequency oscillation. Another important difference from prior work is that the only available phase matching for the crystal ZGP is Type I with  $2.050(o) \rightarrow 3.400(e) + 5.163(e)$ , where wavelengths are in  $\mu\text{m}$  and “o” and “e” denote ordinary and extraordinary waves, and the arrow denotes the direction of energy flow. Other common crystals such as KTP and BBO offer Type II phase matching that often allows selection of pump, signal, and idler polarizations that reduce susceptibility of the OPO’s beam quality to the beam quality of the pump laser. And finally, the pump beam spatial profile in the mid-IR system is not flat-topped but lowest order Gaussian with a  $1/e^2$ -diameter of 4.0–4.5 mm, which results in higher peak fluences for equivalent energy output, and is also usually accompanied by an overall reduction in conversion efficiency. The mid-IR system benefits from a comparatively low  $N_F \approx 30$  but its operating parameters may otherwise diminish performance compared to previous experimental configurations. Nonetheless, we have achieved good results with overall conversion efficiency of approximately 35% as shown in Fig. 5(a), and beam quality that is at most 1.8-times diffraction limited, as shown in Fig. 5(b) and 5(c).

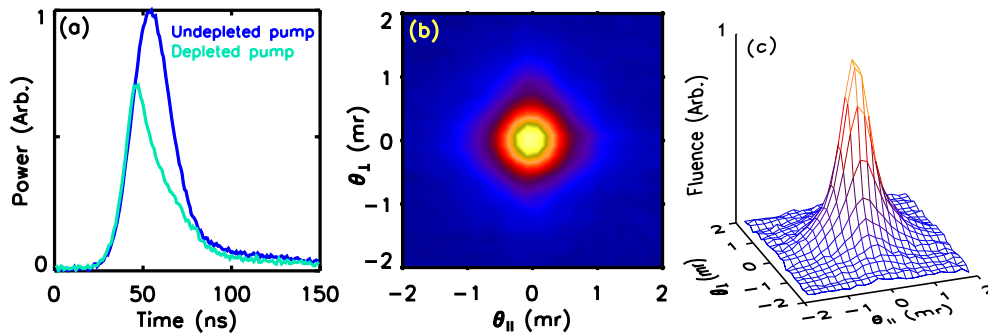


Fig. 5. (a). Depleted and undepleted pump pulse temporal profiles showing  $\sim 35\%$  pump depletion for 3.4- $\mu\text{m}$  signal energy of  $\sim 10$  mJ. Percent pump depletion, defined as  $100 \times (A_{\text{undep}} - A_{\text{dep}}) / A_{\text{undep}}$ , where  $A_{\text{undep}}$  and  $A_{\text{dep}}$  are time-integrated areas for the undepleted and depleted pump pulses, provides a measure of total conversion efficiency. Measurements were obtained from a detector with 1-ns resolution that monitored pump energy after the pump beam passed through the cavity. The undepleted pump pulse was recorded by blocking circulation of the signal inside the OPO cavity. (b) Contour plot of the spatial fluence profile of the 3.4- $\mu\text{m}$  signal beam in the far field plotted against the far-field angles  $\theta_{\parallel}$  and  $\theta_{\perp}$  where  $\parallel$  and  $\perp$  denote directions parallel and perpendicular to birefringent walk-off in the ZGP crystal. The far-field fluence was recorded with a 500-mm focal length lens with effective  $f/\# \approx 140$ . Approximating the diffraction-limited focal-spot diameter by  $\lambda f/\#$  suggests a far-field angular spread of  $< 0.8$  mrad, indicating the signal beam quality exceeds the diffraction limit by at most a factor of 1.8. A rigorous  $M^2$  analysis using second moments from two-dimensional spatial fluence profiles would yield a more accurate value for this factor. Spatial integration of the fluence profile indicates that approximately 14% of the total energy of  $\sim 10$  mJ falls within the diffraction limited spot size, or within  $\pm 0.4$  mrad in the far field. (c) Surface plot of (b).

We do not expect that broadband operation of the mid-IR system will yield optimum results. Currently we are unable to obtain single-frequency oscillation in the laboratory, nor can we accurately simulate broadband oscillation numerically. Therefore we can not quantify discrepancies between the two different operating conditions. Previous single-frequency applications of the RISTRA, and of three-mirror ring cavities, were compared to two-dimensional numerical models that included walk-off and diffraction [16], and the model predictions usually matched measurements within a few percent [17]. A plane wave model for broadband operation of ns OPOs is available but is not capable of predicting performance of real devices with high accuracy [16]. Although a full three-dimensional model that includes birefringent walk-off, diffraction, and image rotation, could be developed for modeling broadband operation of the RISTRA, its memory requirements and computation time would be impractical for desktop computer systems. To obtain a meaningful comparison between laboratory results with existing RISTRA models would require converting the experiment to single-frequency oscillation.

Figure 6 shows experimental input-output measurements for broadband oscillation of ZGP RISTRA OPO. We also show the calculated curve for two-dimensional single-frequency oscillation model for comparison. There is a discrepancy between the measured and calculated curves. We partially attribute the substantial difference in the oscillation thresholds to the absence of a seed laser so that the OPO must start up from quantum fluctuations in the signal and idler fields, but we can also attribute this and other discrepancies to any uncertainty in the value of  $d_{\text{eff}}$  for ZGP, and to the various physical mechanisms described below.

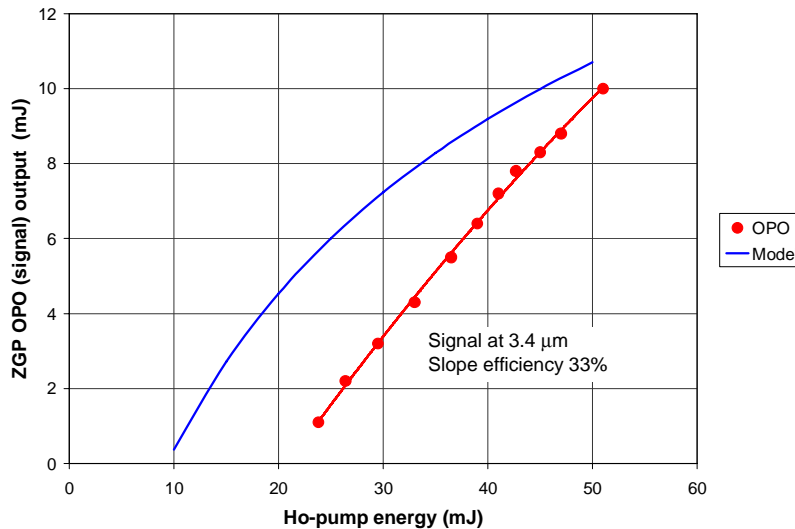


Fig. 6. Measured and calculated efficiency curves showing OPO signal energy at 3.4  $\mu\text{m}$  versus 2.05- $\mu\text{m}$  pump energy. The calculated curve was obtained from a two-dimensional model for the RISTRA OPO that assumes a single-frequency pump laser and single-frequency oscillation in the OPO, and includes birefringent walk-off, diffraction, and image rotation. Measured performance is for a broadband pump laser with a free running OPO. With the broadband pump and oscillation, the signal linewidth was measured to be slightly less than 40 nm near 3.4  $\mu\text{m}$ . The difference in the oscillation thresholds can be partially attributed to start-up from quantum fluctuations in the signal and idler fields for the laboratory measurements, opposed to start-up using an injection seeding source in the model. Additional discrepancies can be attributed to uncertainty in the value of effective nonlinearity,  $d_{\text{eff}}$ , used for ZGP in the calculations, and to the various physical mechanisms described in the text. For these calculated and measured results, the length of the ZGP crystal is 10 mm and the pump  $1/e^2$ -diameter 4.0–4.5 mm. The output coupler reflectivity is  $\sim 50\%$ .

The measured average power of the RISTRA OPO 3.4- $\mu\text{m}$  signal wave and 2- $\mu\text{m}$  pump vs the repetition rate is shown in Fig. 7. By adjusting the Tm-fiber laser pump the pulse energy from the Ho:YLF-MOPA was maintained exactly at 50 mJ for each repetition rate. As one can see from Fig.7 the average power of the OPO signal wave does increase linearly with the increasing repetition rate. This confirms that the OPO performance is not affected by the thermal effects at pump average power of up to 25 W.

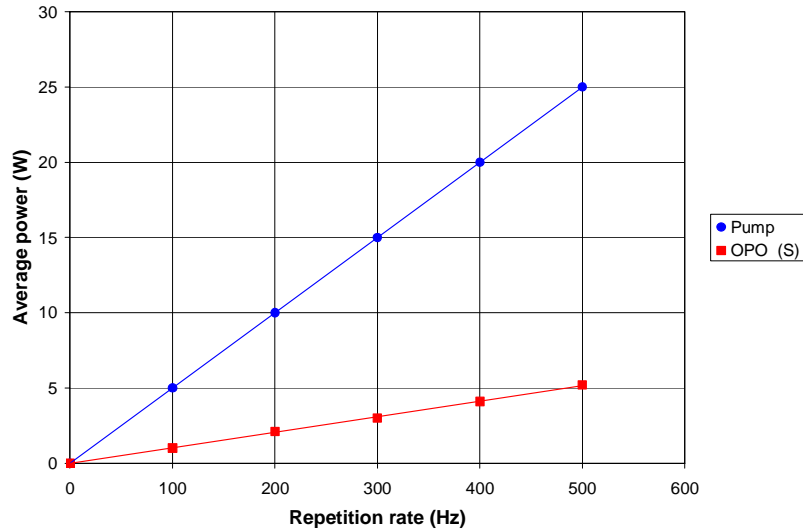


Fig. 7. Measured average power of the RISTRA OPO 3.4- $\mu\text{m}$  signal wave and 2- $\mu\text{m}$  pump vs the repetition rate. Pump pulse energy was set at 50 mJ for each repetition rate. The average power of the OPO signal wave does increase linearly with the increasing repetition rate. This shows that OPO performance is not affected by the thermal effects at pump average power of up to 25 W.

Broadband oscillation in ns OPOs can diminish performance for the following reasons. For homogeneously broadened laser gain media such as Ho:YLF, the temporal structure of the pump pulse due to cavity mode beating results in nonlinear mixing with complex temporal dynamics. This is especially true for the spatially non-uniform Gaussian pump profile, where irradiance-dependent effects like parametric back-conversion occur with unequal strength across the beam profile. Back-conversion reduces conversion efficiency and also reduces beam quality, especially for non-uniform pump-beam spatial profiles [18]. Another subtle effect of broadband oscillation involves the longitudinal mode structure of non-planar ring cavities. With  $90^\circ$  of intra-cavity image rotation per cavity pass, the RISTRA supports off-axis longitudinal modes that close after as many as  $360^\circ/90^\circ = 4$  passes around the cavity. Two of these modes are charge  $\pm 1$  optical vortices and a single two-times around mode is a charge 2 vortex, with the three additional modes non-degenerated in frequency and each separated by  $1/4$  of the cavity's free spectral range of  $\sim 2.75$  GHz [19]. Broadband oscillation occurs predominantly for the RISTRA's one-time around mode, where gain is greatest. However, with the Ho:YLF pump laser's estimated bandwidth of  $> 10$   $\text{cm}^{-1}$  (300 GHz), and free-running oscillation in the OPO, many of these off-axis modes can be excited so that the higher-gain one-time around mode does not deplete all of the energy in the pump pulse. Even when the one-time around mode is selected by injection seeding, a very small fraction of the total energy can be contained in the off-axis modes. For example, with increasing  $N_F$  there is an observable shoulder in the far-field spatial fluence profile for the OPO's resonated wave that may be partially attributed to these modes. For broadband oscillation, the energy in this shoulder usually increases. In addition, there are observable fluctuations in the shape and amplitude of the shoulder due to shot-to-shot variations in the admixture of these modes,



especially for pump energies near the oscillation threshold. Although these effects are subtle, they are enhanced by broadband oscillation and can reduce beam quality and conversion efficiency. As we do not have the data for single-frequency operation of ZGP RISTRA OPO we show the comparison of far-field signal spatial fluence profiles in Fig. 8 for single-frequency oscillation, and broadband oscillation, for a 0.532- $\mu\text{m}$ -pumped KTP RISTRA OPO which clearly illustrates the increase in the size of the shoulder. In Fig. 8(a) the pump laser and OPO are each injection-seeded, whereas in Fig. 8(b) neither is injection-seeded. Note the similarities in the shapes of the far-field fluence profiles for broadband oscillation in Fig. 8(b) and in Fig. 5(c).

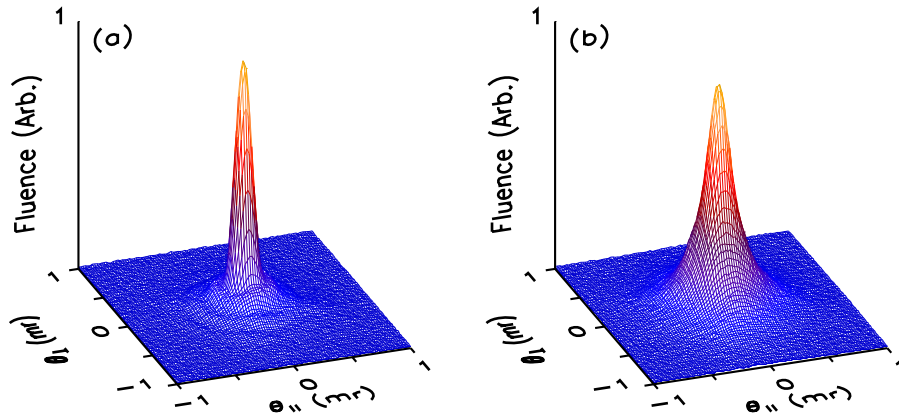


Fig. 8. (a) Far field signal spatial fluence profile for a one-crystal KTP RISTRA OPO where the Nd:YAG pump laser and OPO are each injection-seeded for single-frequency oscillation. The mixing in  $xz$ -cut KTP is  $0.532(o) \rightarrow 0.800(e) + 1.588(o)$ . The pump beam diameter was  $\sim 5$  mm and its spatial fluence profile was globally flat-topped but contained ring-like modulation due to hard apertures from overfilled laser amplifier rods. The OPO's injection-seeded oscillation threshold was 23 mJ and the pump energy was  $4\times$  the threshold. In contrast to the mid-IR system, the cavity Fresnel number for the KTP RISTRA is approximately 200, and the diffraction-limited focal-spot diameter and corresponding far-field angular spread are respectively  $100 \mu\text{m}$  and  $200 \mu\text{rad}$ . Approximately 24% of the total  $0.800\text{-}\mu\text{m}$  signal energy falls within  $\pm 0.1$  mrad. (b) Far field signal fluence for the same experimental conditions as in (a) except the pump laser and OPO are now unseeded for broadband oscillation. The small reduction in peak height in the far field is real, and is accompanied by a reduction in conversion efficiency when compared to single-frequency oscillation. Now approximately only 13% of the total signal energy falls within  $\pm 0.1$  mrad, consistent with the results for broadband oscillation in Fig. 5.

While broadband oscillation reduces beam quality, it may also affect Poynting vector stability for the entire beam, although the position of the central peak in the far field should be stable. Analysis of pointing stability for the  $3.4\text{-}\mu\text{m}$  signal wave of the mid-IR system reveals shot-to-shot variations as high as  $15 \mu\text{rad}$ , but this measurement was influenced by noise in the camera system (Spiricon Pyrocam-III). Averaging 10 consecutive camera frames reduces pointing stability to approximately  $6 \mu\text{rad}$ , but this is still high compared to previous measurements. Centroid analysis of pulse injection-seeded operation in Ref. [12], where the signal wavelength was  $803 \text{ nm}$  and  $N_F$  was  $\geq 400$  revealed pointing stability of  $\leq 2.5 \mu\text{rad}$ . Although a comparison with single-frequency oscillation is not currently possible with the mid-IR system, it is reasonable to expect that the additional mode structure introduced by broadband oscillation influences these measurements.

Another important difference between the mid-IR system and previous RISTRA applications involves phase matching in ZGP. Singly-resonant OPOs typically achieve their best beam quality when the resonant wave – usually the signal – is least susceptible to undesirable influences from the pump or idler waves. This condition can be achieved by

selecting mixing so that the pump and idler share the same polarization and co-propagate. For example, in Ref. [12] we used  $0.532(o) \rightarrow 1.576(o) + 0.803(e)$  in  $xz$ -cut KTP where the 0.532- $\mu\text{m}$  pump and 1.576- $\mu\text{m}$  idler shared o-polarization, while the e-polarized signal – which walks off from the idler and pump – was a mode of the cavity. Switching polarizations so that  $0.532(e) \rightarrow 1.576(e) + 0.803(o)$  would also work well, but using  $0.532(e) \rightarrow 1.576(o) + 0.803(e)$ , where the pump and signal co-propagate, would make the resonated signal more susceptible to the beam quality of the pump. ZGP offers only  $2.050(o) \rightarrow 3.400(e) + 5.163(e)$  where the e-polarized signal and idler waves share near identical refractive indices and co-propagate. While this mixing should reduce susceptibility of the signal to the beam quality of the pump, the signal can be influenced by the idler. Four mirror reflections for each pass around the signal-resonant one-crystal configuration should eliminate any influence from the idler. However in a two-crystal ZGP RISTRA cavity, where there would be only two mirror reflections between crystals, any undesirable influence from the non-resonant idler may increase.

## 7. Conclusion

We have demonstrated a broadband operation of ZGP OPO utilizing the RISTRA concept. The 3D image-rotating resonator with birefringent mode cleaning produced a signal OPO beam with almost diffraction-limited beam quality. We achieved 10 mJ in signal-wave output from the ZGP OPO with ~55 mJ pump pulse energy. In principle, the ZGP RISTRA OPO design can operate at pump pulse energy of up to 250 mJ to produce higher energy in the signal wave. The OPO efficiency can be increased by utilizing the flat-topped pump beam profile and switching into single-frequency regime.